GEOPHYSICS, VOL. 55, NO. 6 (JUNE 1990); P. 734–748, 16 FIGS.

Solution of the equations of dynamic elasticity by a Chebychev spectral method

D. Kosloff*, D. Kessler‡, A. Q. Filho§, E. Tessmer**, A. Behle§, and R. Strahilevitz‡

ABSTRACT

We present a spectral method for solving the two-dimensional equations of dynamic elasticity, based on a Chebychev expansion in the vertical direction and a Fourier expansion for the horizontal direction. The technique can handle the free-surface boundary condition more rigorously than the ordinary Fourier method.

The algorithm is tested against problems with known analytic solutions, including Lamb's problem of wave propagation in a uniform elastic half-space, reflection from a solid-solid interface, and surface wave propagation in a half-space containing a low-velocity layer. Agreement between the solutions is very good. A fourth example of wave propagation in a laterally heterogeneous structure is also presented. Results indicate that the method is very accurate and only about a factor of two slower than the Fourier method.

INTRODUCTION

This work presents a spectral method for the solution of the equations of dynamic elasticity in two spatial dimensions. The method is based on a spatial discretization on a grid in which the solution is approximated by a Chebychev expansion in the vertical direction and a Fourier method in the horizontal direction. This discretization yields an algorithm with spectral accuracy which is not periodic in the vertical direction. Consequently, unlike the Fourier method, the free-surface boundary condition can be incorporated easily.

The problem of expressing the free-surface boundary condition with grid methods is not always simple. The free-surface boundary condition is especially difficult with high-order schemes. Whereas for finite elements or low-order finite differences the free-surface condition can be applied with the same level of accuracy as the method itself (e.g., Vidale and Clayton, 1986), for the fourth-order finite differences only an approximation to the condition has been found (Baylis et al., 1986; Levander, 1988). Furthermore, for the spectrally accurate Fourier method we had to resort to "zero padding," effectively including a region above the surface of the earth with a velocity value of zero (Kosloff et al., 1984). Whereas for small angles of incidence (or, equivalently, at a large depth beneath the surface) this approximation yields acceptable results, for larger angles of incidence the time histories become ringy. An example of this behavior is shown in Figures 1a and 1b which present comparisons between the Fourier method and analytical solutions for Lamb's problem of wave propagation in a homogeneous half-space. In this example the source was located at a depth of 20 m beneath the free surface and had a Ricker wavelet time history with peak frequency at 11 Hz. The P-wave and S-wave velocities were, respectively, 2000 m/s and 1155 m/s. Figure 1a, which presents horizontal displacements on the surface at a distance of 1200 m from the source, appears ringy. Conversely, the comparison between numerical and analytical results in Figure 1b, which is for a point located at a depth of 400 m beneath the surface in the same horizontal position, is much better.

The free-surface boundary condition is important for exploration geophysics. First, an accurate representation of the seismic source must account for reflected and converted phases from the surface. Second, evaluating ground roll and wave propagation in the weathered zone in general is important. We therefore believe it is desirable to have a modeling scheme which can handle these phenomena accurately. In this study we examine the possibility of using an algorithm based on a Chebychev expansion in the vertical direction.

Manuscript received by the Editor June 28, 1988; revised manuscript received October 2, 1989.
*Department of Geophysics and Planetary Sciences, Tel Aviv University, Tel Aviv, Israel 69978; and Geophysical Institute, Hamburg University, D-2000 Hamburg, West Germany.
‡Department of Geophysics and Planetary Sciences, Tel Aviv University, Tel Aviv, Israel 69978.
§PPPG Inst. Geosci., Universidade Federal da Bahia, Federacao, Salvador, Bahia, Brazil.
**Geophysical Institute, Hamburg University, D-2000 Hamburg, West Germany.

The Chebychev method has been described extensively in the mathematical literature (e.g., Gottlieb and Orszag, 1977; Canuto et al., 1987, for a review). As with the Fourier method and finite differences, the algorithm uses a spatial mesh to approximate the solution. However, the grid is no longer uniform in the vertical direction, but rather is finer toward the boundaries (Figure 2). The degree of refinement of the mesh toward the boundaries is controlled by a mapping into another coordinate system. Since numerical stability depends on the size of the smallest grid spacing, this mapping enables one to achieve a proper balance between fulfillment of the surface boundary conditions and numerical efficiency. As we show, the method accounts for the free-surface boundary condition and is very accurate. It is also comparable in speed to the ordinary Fourier method.

In the following sections we describe the Chebychev modeling scheme and discuss its properties. We next present a comparison between numerical and analytical calculations for problems with known solutions and an example of wave propagation in a laterally heterogeneous medium.

EQUATIONS OF DYNAMIC ELASTICITY

The numerical algorithm is based on a solution of the equations of conservation of momentum combined with the stress-strain relation for an isotropic elastic solid undergoing infinitesimal deformation (e.g., Fung, 1965). For two spatial dimensions the equations of momentum conservation are given by

$$\rho\ddot{u}_x = \frac{\partial\sigma_{xx}}{\partial x} + \frac{\partial\sigma_{xy}}{\partial y} + f_x$$
$$\rho\ddot{u}_y = \frac{\partial\sigma_{xy}}{\partial x} + \frac{\partial\sigma_{yy}}{\partial y} + f_y, \tag{1}$$

where x and y are the horizontal and vertical coordinates, respectively, u_x and u_y are the horizontal and vertical displacement components, σ_{xx}, σ_{xy}, and σ_{yy} are the stresses, f_x and f_y are the body forces per unit volume, and ρ denotes the density. In equation (1) as in the remainder of this work a dot above a variable denotes time differentiation.

The stress-strain relation for an isotropic elastic solid expressed in terms of displacement derivatives reads

$$\sigma_{xx} = (\lambda + 2\mu)\frac{\partial u_x}{\partial x} + \lambda\frac{\partial u_y}{\partial y}$$
$$\sigma_{yy} = \lambda\frac{\partial u_x}{\partial x} + (\lambda + 2\mu)\frac{\partial u_y}{\partial y} \tag{2}$$

and

$$\sigma_{xy} = \mu\left[\frac{\partial u_x}{\partial y} + \frac{\partial u_y}{\partial x}\right],$$

where λ and μ are, respectively, the rigidity and the shear modulus.

Equations (1) and (2) are sufficient to determine the deformation history of the body once boundary conditions have been specified. For the earth's surface, the condition is of zero traction. Assuming a flat surface and with our choice of coordinates, this condition reads

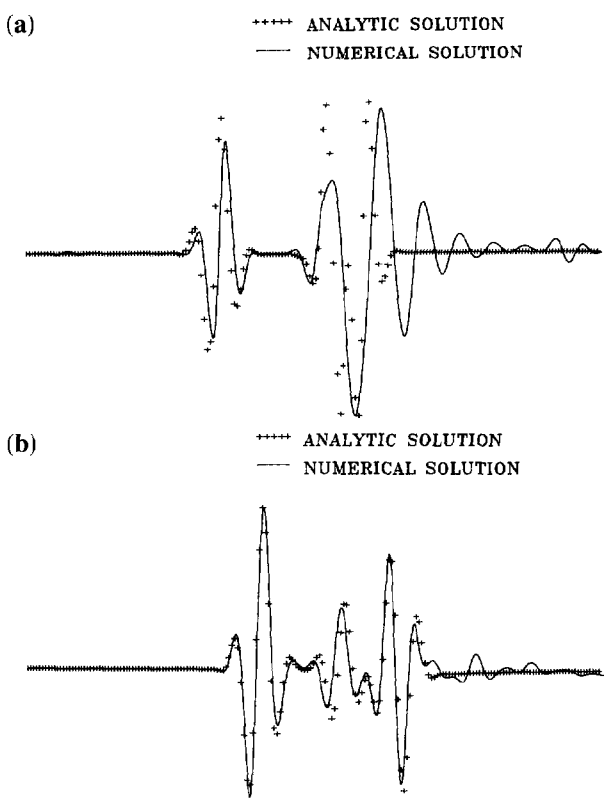

FIG. 1. Comparison between the Fourier and exact solutions for Lamb's problem with a source depth of 20 m and *P*-wave and *S*-wave velocities of 2000 m/s and 1155 m/sec, respectively. (a) Geophone located at horizontal distance of 1200 m at the surface. (b) Geophone located at horizontal distance 1200 m at a depth of 400 m beneath the surface.

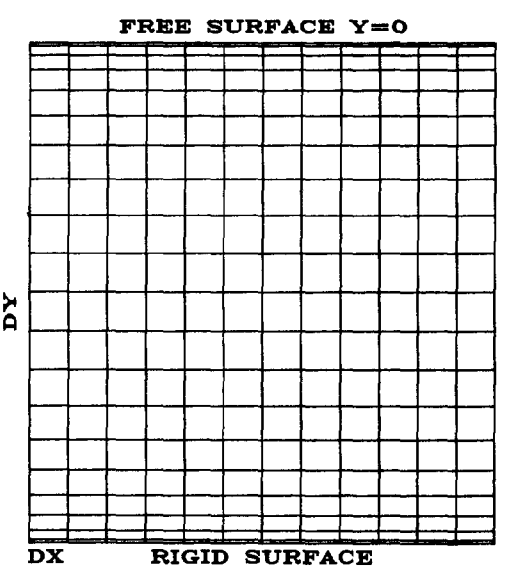

FIG. 2. Typical mesh for the Chebychev algorithm.

$$\sigma_{xy} = 0$$
$$\sigma_{yy} = 0 \tag{3}$$

For the numerical algorithm described in this study, equations (1) and (2) are recast as a system of five coupled first-order equations given by

$$\frac{\partial}{\partial t}\begin{bmatrix} \dot{u}_x \\ \dot{u}_y \\ \sigma_{xx} \\ \sigma_{yy} \\ \sigma_{xy} \end{bmatrix} = \underline{\mathbf{A}}\begin{bmatrix} \dot{u}_x \\ \dot{u}_y \\ \sigma_{xx} \\ \sigma_{yy} \\ \sigma_{xy} \end{bmatrix}_x + \underline{\mathbf{B}}\begin{bmatrix} \dot{u}_x \\ \dot{u}_y \\ \sigma_{xx} \\ \sigma_{yy} \\ \sigma_{xy} \end{bmatrix}_y + \begin{bmatrix} f_x/\rho \\ f_y/\rho \\ 0 \\ 0 \\ 0 \end{bmatrix}, \tag{4}$$

where

$$\underline{\mathbf{A}} = \begin{bmatrix} 0 & 0 & 1/\rho & 0 & 0 \\ 0 & 0 & 0 & 0 & 1/\rho \\ \lambda + 2\mu & 0 & 0 & 0 & 0 \\ \lambda & 0 & 0 & 0 & 0 \\ 0 & \mu & 0 & 0 & 0 \end{bmatrix} \tag{5}$$

and

$$\underline{\mathbf{B}} = \begin{bmatrix} 0 & 0 & 0 & 0 & 1/\rho \\ 0 & 0 & 0 & 1/\rho & 0 \\ 0 & \lambda & 0 & 0 & 0 \\ 0 & \lambda + 2\mu & 0 & 0 & 0 \\ \mu & 0 & 0 & 0 & 0 \end{bmatrix}. \tag{6}$$

This is the same system as used in Levander (1988), Virieux (1986), and Bayliss et al. (1986) (after correction of typographical errors).

THE SOLUTION SCHEME

The numerical algorithm solves equation (4) subject to the boundary conditions (3). The seismic source is introduced through the body force term. The variables are discretized on a spatial grid which is uniform in the x direction and nonuniform in the y direction (Figure 2). The grid points in the y direction are calculated by a mapping $y_j = y_j(z_j)$ from the Chebychev sampling points $z_j = \cos(\pi j/N), j = 0, \ldots N$, with $N + 1$ the number of grid points in the y direction. (This mapping is discussed in a later section.) Equation (4) contains both spatial and temporal derivatives. For advancing the solution in time, we use a fourth-order Runge-Kutta method. Horizontal derivatives are calculated by the Fourier method (Gazdag, 1981; Kosloff and Baysal, 1982). For the vertical derivatives we use a discrete Chebychev expansion and the recursion relation for the coefficients of the derivative (Gottlieb and Orszag, 1977). The advantage of this expansion is that it can be calculated via a variant of the fast Fourier transform (FFT) for the cosine transform (Gottlieb and Orszag, 1977; Press et al., 1986). For completeness, we summarize below the main details of the Chebychev derivative approximation.

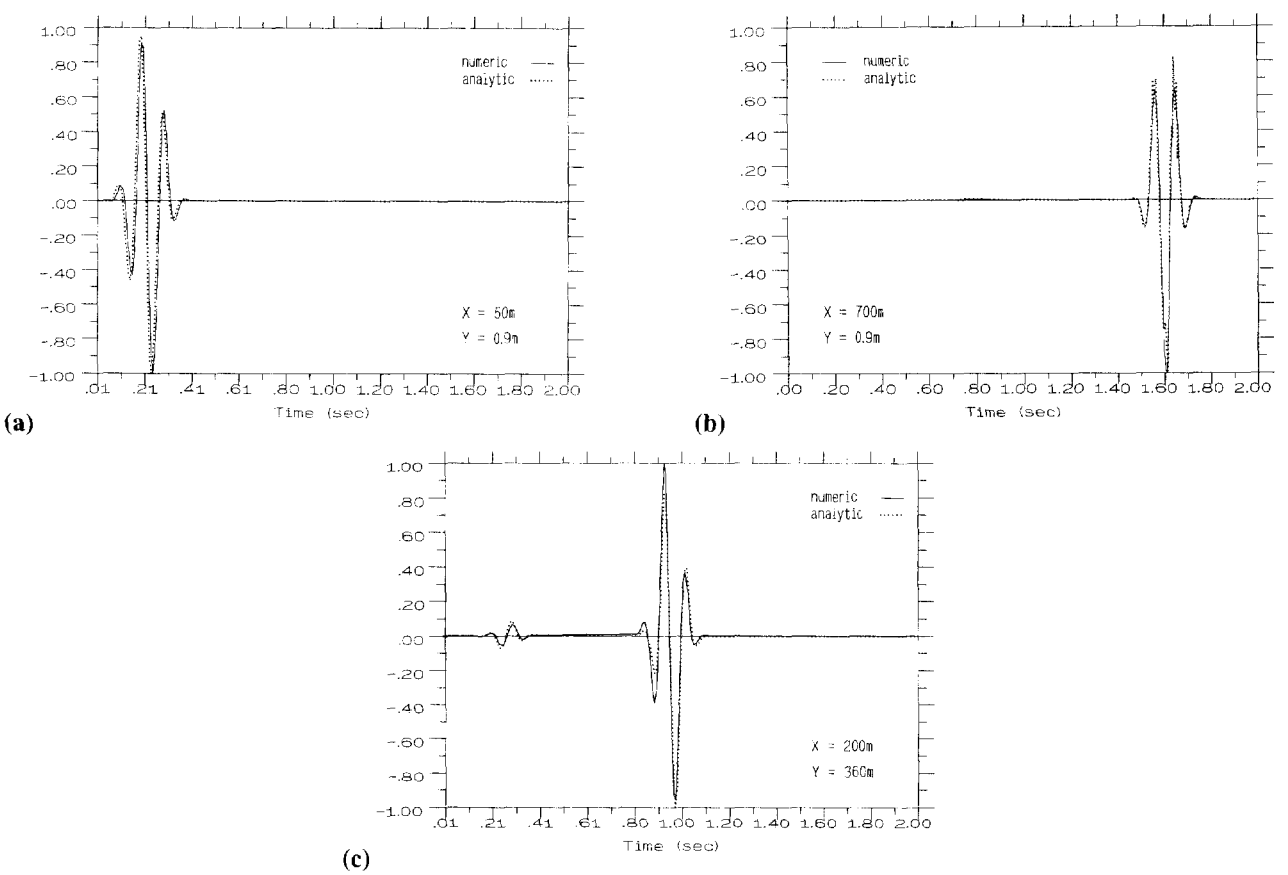

FIG. 3. Comparisons between numerical and analytical horizontal displacement solutions for Lamb's problem (a) at a horizontal distance of 50 m from the source at a depth of 0.9 m, (b) at a horizontal distance of 700 m from the source at a depth of 0.9 m, and (c) at a horizontal distance of 200 m from the source at a depth of 360 m.

We consider a finite piecewise continuous function $f(z)$ where $-1 \le z \le 1$ (results for a different interval can be obtained after scaling). When the sampling points are $z_j = \cos(\pi/N)j$, with $j = 0 \ldots N$, the discrete Chebychev expansion of $f(z)$ is given by

$$f(z_j) = \sum_{k=0}^{N} a_k T_k(z_j), \qquad j = 0, \ldots, N \tag{7}$$

(Hamming, 1978). The coefficients a_k are given by the discrete transform

$$a_k = \frac{2}{N} \sum_{j=0}^{N} \alpha_j f(z_j) I_k(z_j) \begin{cases} 1, & k \neq 0 \\ \frac{1}{2}, & k = 0, \text{ or } N, \end{cases} \tag{8}$$

where

$$a_j = \begin{cases} \frac{1}{2}, & j = 0, \text{ or } N \\ 1, & \text{otherwise} \end{cases}$$

(Hamming, 1978). As with the discrete Fourier transform, the coefficients a_k match the coefficients of the continuous Chebychev expansion when the function $f(z)$ is band-limited. Here the band limitedness is in the sense that the function should be expressible as a polynomial of order up to N.

Assuming $f(z)$ is band-limited, its derivative can be expanded by

$$\frac{df(z_j)}{dz} = \sum_{k=0}^{N} b_k T_k(z_j), \qquad j = 0, \ldots, N. \tag{9}$$

The coefficients b_k are related to the coefficients a_k in equation (8) by the downward recursion relation

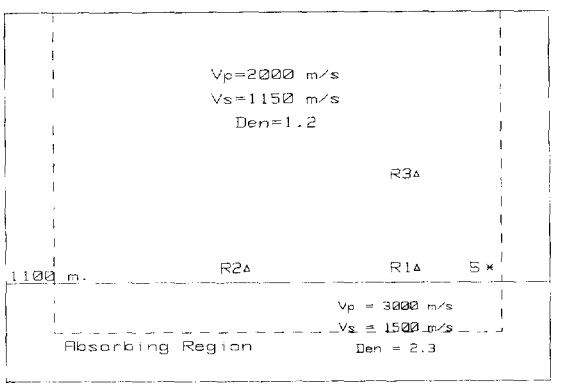

FIG. 5. Grid configurations for the problem of two solids in planar contact.

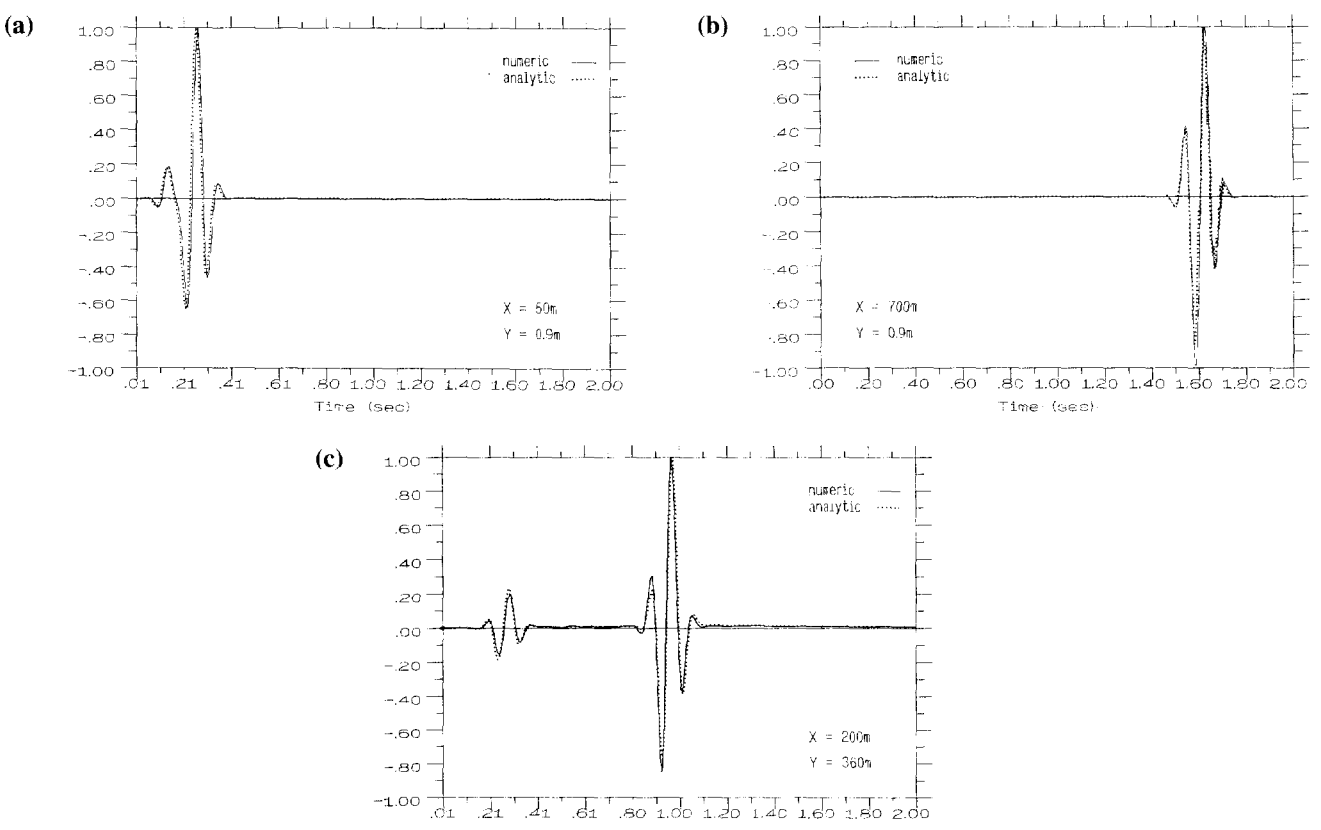

FIG. 4. Comparisons between numerical and analytical vertical displacement solutions for Lamb's problem (a) at a horizontal distance of 50 m from the source at a depth of 0.9 m, (b) at a horizontal distance of 700 m from the source at a depth of 0.9 m, and (c) at a horizontal distance of 200 m from the source at a depth of 360 m.

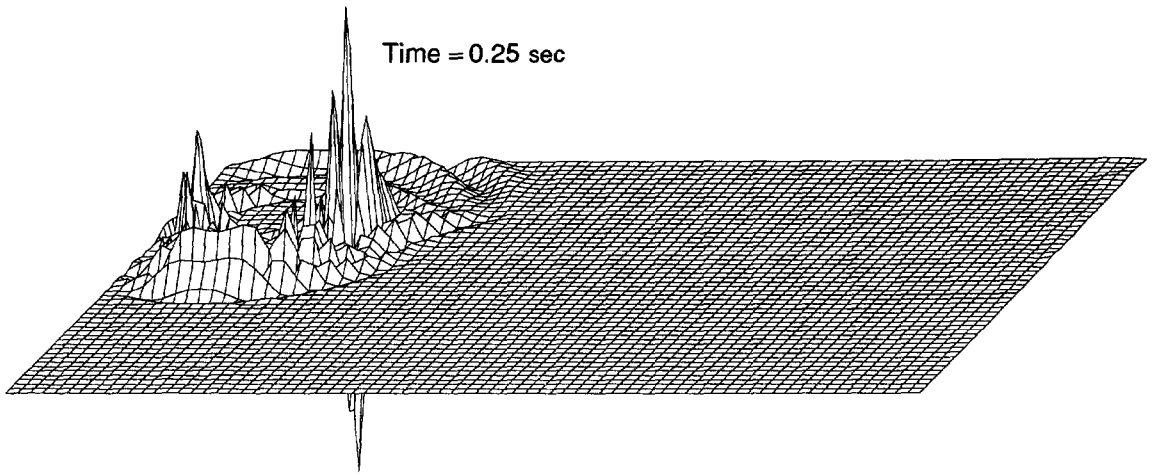

(a)

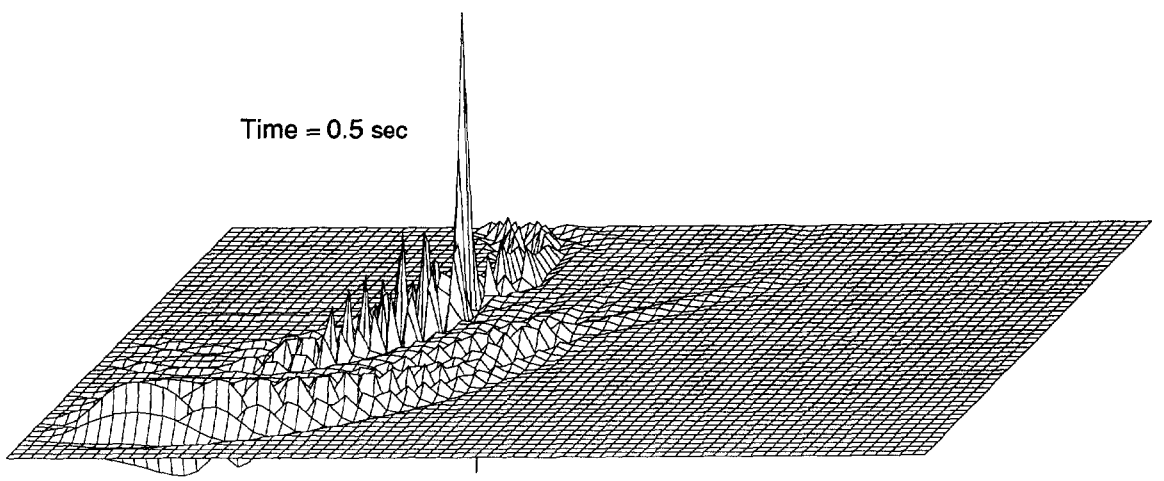

(b)

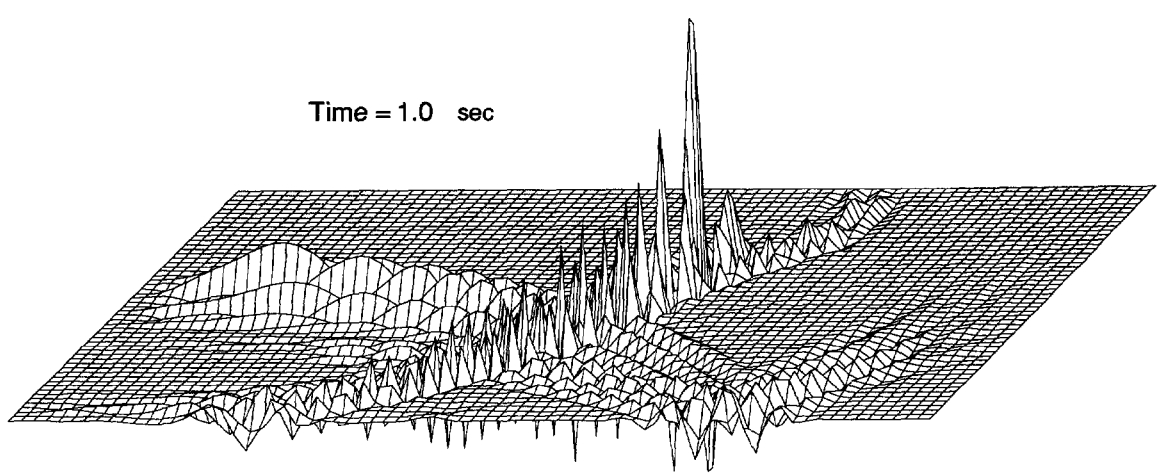

(c)

FIG. 6. Vertical particle velocity snapshots for the two solids problem at times: (a) $t = 0.25$ s, (b) $t = 0.5$ s, and (c) $t = 1$ s.

$$b_{k-1} = b_{k+1} + 2ka_k, \qquad k = N, \ldots, 2, \qquad (10)$$

and

$$b_0 = \frac{2a_1 + b_2}{2},$$

with starting values $b_{N+1} = b_N = 0$ (Gottlieb and Orszag, 1977).

Relations (7), (8), (9), and (10) allow the calculation of a Chebychev derivative approximation. Given a sampled function $f(z_j)$, the coefficients a_k can be calculated from equation (8) by a variant of the FFT (Gottlieb and Orszag, 1977; Press et al., 1986). Then the coefficients b_k can be calculated by equation (10). The derivative df/dz is finally obtained after a transform of the coefficients b_k according to equation (9). The computational effort of the whole process is comparable to the effort in the Fourier derivative approximation (e.g., Kosloff and Baysal, 1982).

BOUNDARY CONDITIONS

The free-surface boundary condition requires zero values for σ_{xy} and σ_{yy} on the surface $y = 0$. However, as was shown in Gottlieb et al. (1982) and Bayliss et al. (1986), direct application of this condition without regard to the other variables $\dot{u}_x$, $\dot{u}_y$, and σ_{xx} can lead to numerical instability. Stabilization can be achieved by requiring that outgoing characteristic variables remain unmodified after application of the boundary conditions (Gottlieb et al., 1982). For the free-surface boundary condition at $y = 0$ this implies

$$\dot{u}_x^{(\text{new})} = \dot{u}_x^{(\text{old})} + \frac{1}{\rho v_s}\sigma_{xy}^{(\text{old})}$$

$$\dot{u}_y^{(\text{new})} = \dot{u}_y^{(\text{old})} + \frac{1}{\rho v_p}\sigma_{yy}^{(\text{old})}$$

and

$$\sigma_{xx}^{(\text{new})} = \sigma_{xx}^{(\text{old})} - \frac{\lambda}{(\lambda + 2\mu)}\sigma_{yy}^{(\text{old})}$$

(Bayliss et al., 1986), where v_p and v_s denote the p and s velocities respectively. The superscripts (old) and (new) denote values of variables before and after application of the boundary condition, respectively. Thus in a typical calculation, first the operator on the right-hand side of equation (4) acts on a vector of variables $(\dot{u}_x, \dot{u}_y, \sigma_{xx}, \sigma_{yy}, \sigma_{xy})^T$ to yield an output vector which is then updated according to the procedure above.

For the boundary at the bottom of the grid we use the

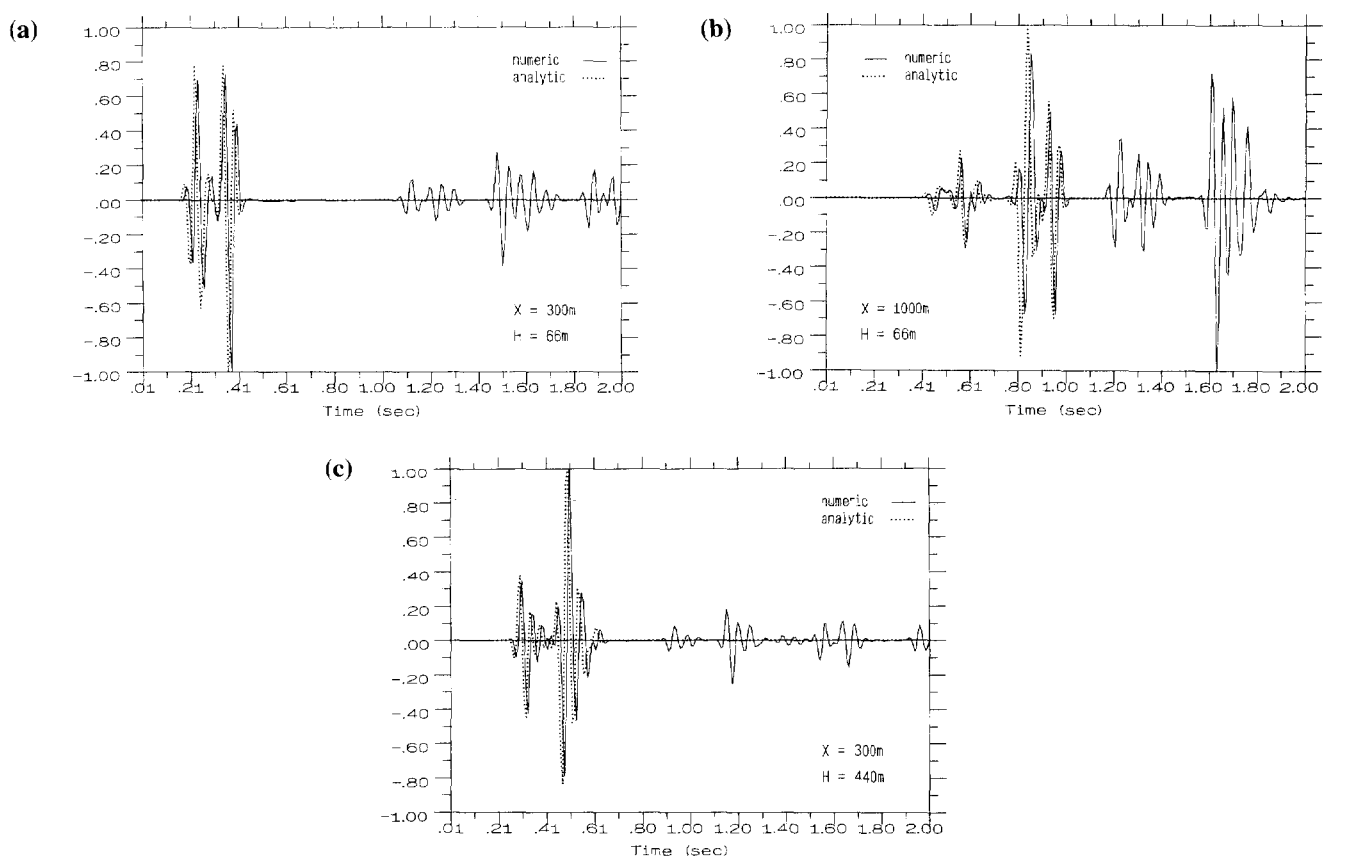

FIG. 7. Comparisons between numerical and analytical horizontal displacement solutions for the two-solids problem (a) at a horizontal distance of 300 m from the source at a height of 66 m above the interface, (b) at a horizontal distance of 1000 m from the source at a height of 66 m above the interface, and (c) at a horizontal distance of 300 m from the source at a height of 440 m above the interface.

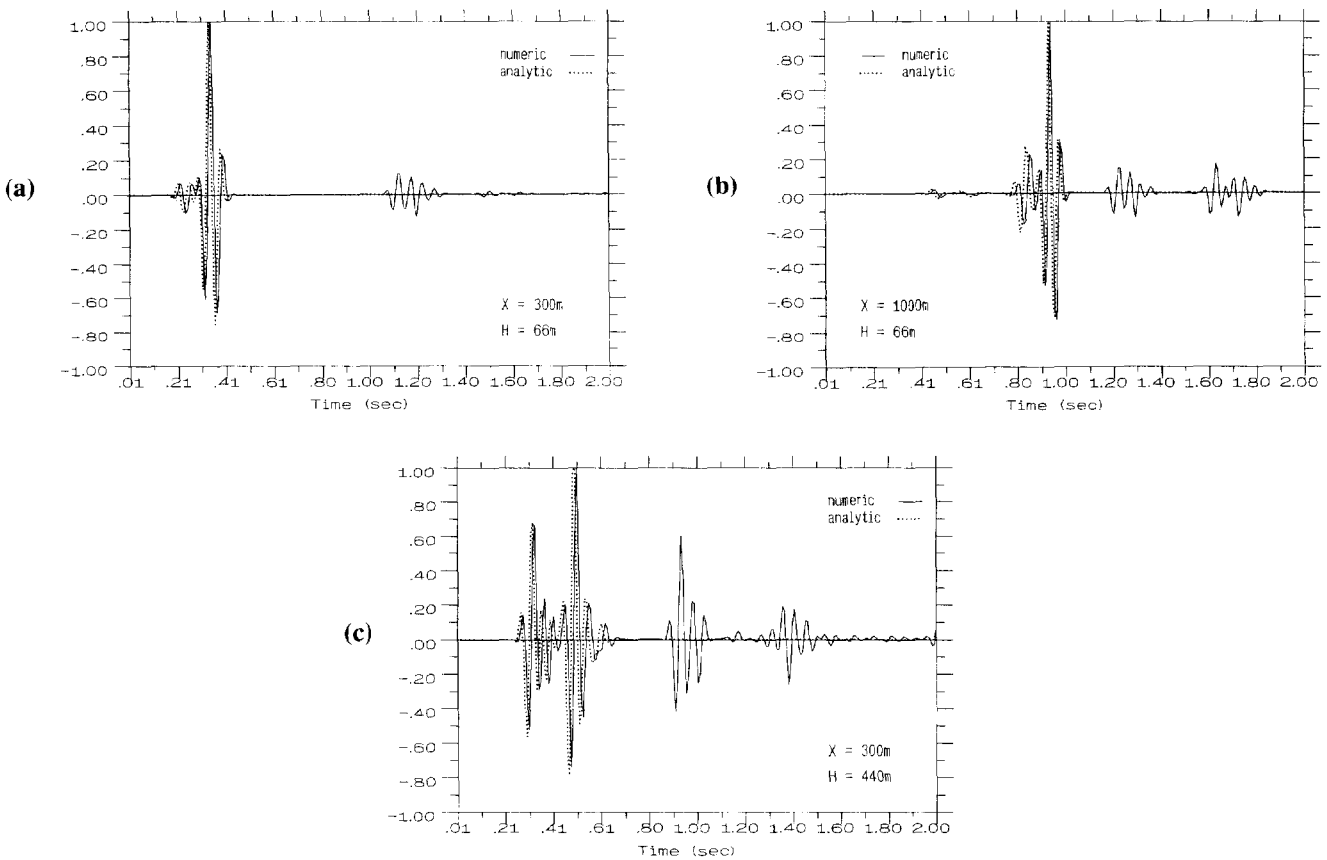

FIG. 8. Comparisons between numerical and analytical vertical displacement solutions for the two-layer problem (a) at a horizontal distance of 300 m from the source at a height of 66 m above the interface, (b) at a horizontal distance of 1000 m from the source at a height of 66 m above the interface, and (c) at a horizontal distance of 300 m from the source at a height of 440 m above the interface.

nonreflecting condition described in Bayliss et al. (1986). The corresponding procedure reads

$$\sigma_{xy}^{(\text{new})} = 0.5\,[\sigma_{xy}^{(\text{old})} - \rho v_s \dot{u}_x^{(\text{old})}],$$

$$\dot{u}_x^{(\text{new})} = 0.5\,[\dot{u}_x^{(\text{old})} - \sigma_{xy}^{(\text{old})}/\rho v_s],$$

$$\sigma_{yy}^{(\text{new})} = 0.5\,[\sigma_{yy}^{(\text{old})} - \rho v_p \dot{u}_y^{(\text{old})}],$$

$$\dot{u}_y^{(\text{new})} = 0.5\,[\dot{u}_y^{(\text{old})} - \sigma_{yy}^{(\text{old})}/\rho v_p],$$

$$\sigma_{xx}^{(\text{new})} = \sigma_{xx}^{(\text{old})} + \frac{\lambda}{\lambda + 2\mu}\,[\sigma_{yy}^{(\text{new})} - \sigma_{yy}^{(\text{old})}].$$

This condition reduces reflections from the bottom of the grid; however, it does not eliminate them completely (particularly for nonvertical angles of incidence). An absorbing region was added along the sides and bottom of the grid to prevent wraparound and boundary reflections (Cerjan et al., 1985; Kosloff and Kosloff, 1986).

IMPROVEMENT OF STABILITY THROUGH A COORDINATE TRANSFORMATION

As in all grid methods, the Chebychev mesh should be chosen fine enough to resolve all wavenumber components in the problem. Furthermore, the boundary conditions need to be represented accurately. Experience and sampling considerations indicate that the grid spacing in the center of the mesh should be chosen smaller than half the shortest wavelength component in the propagating pulses. Thus the grid needs to be scaled from [−1, 1] to the actual dimension of the problem. However when the mesh size is doubled with the Chebychev method, the grid spacing in the vicinity of the boundary decreases by a factor of two (or by a factor of four

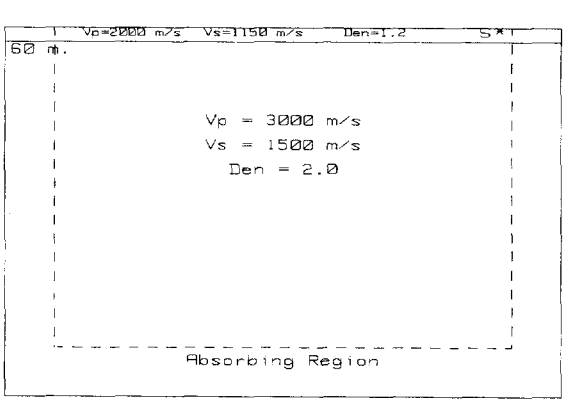

FIG. 9. Grid configuration for the thin-layer problem.

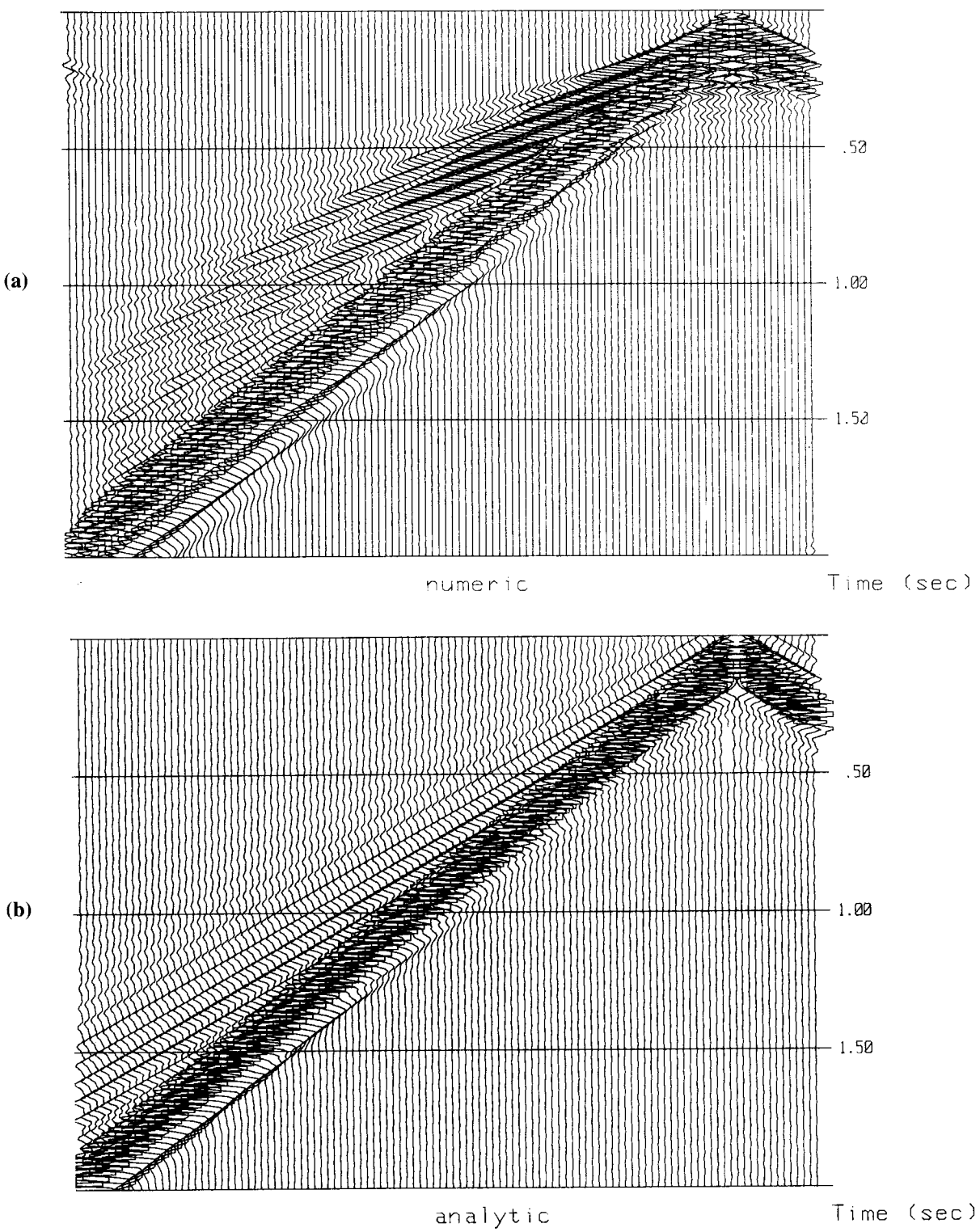

FIG. 10. (a) Horizontal displacement time section calculated numerically for the thin-layer problem at a depth of 0.9 m. (b) Horizontal displacement time section calculated analytically for the thin-layer problem at a depth of 0.9 m.

in the original grid before scaling). This is unlike with finite differences or the Fourier method where the grid spacing remains constant. The stable time step size decreases accordingly, thus making the Chebychev method prohibitively expensive. To circumvent this problem, we introduce a coordinate transformation by which the grid spacing in the vicinity of the boundary remains practically constant for different grid sizes, and yet is small enough to resolve the boundary conditions properly. This coordinate transformation is discussed in more detail in Kosloff and Tal-Ezer (1989).

Let z denote the coordinate of the original Chebychev mesh spanning the region $[-1, 1]$ and y a coordinate system which is obtained from the z system by a transformation $y = y(z)$. Given a function $f(y)$, its derivative can be calculated by the chain rule

$$\frac{df}{dy} = \frac{df}{dz}\frac{dz}{dy},$$

where df/dz can be calculated via the FFT as previously explained. For the transformation $y = y(z)$, we chose

$$y(z) = \frac{-1}{\sqrt{|c|}} \arcsin\left(\frac{2cz + b}{\sqrt{b^2 - 4c}}\right),$$

where

$$b = 0.5\ \alpha^{-2}\ (\beta^{-2} - 1)$$

and

$$c = 0.5\ \alpha^{-2}\ (\beta^{-2} + 1) - 1.$$

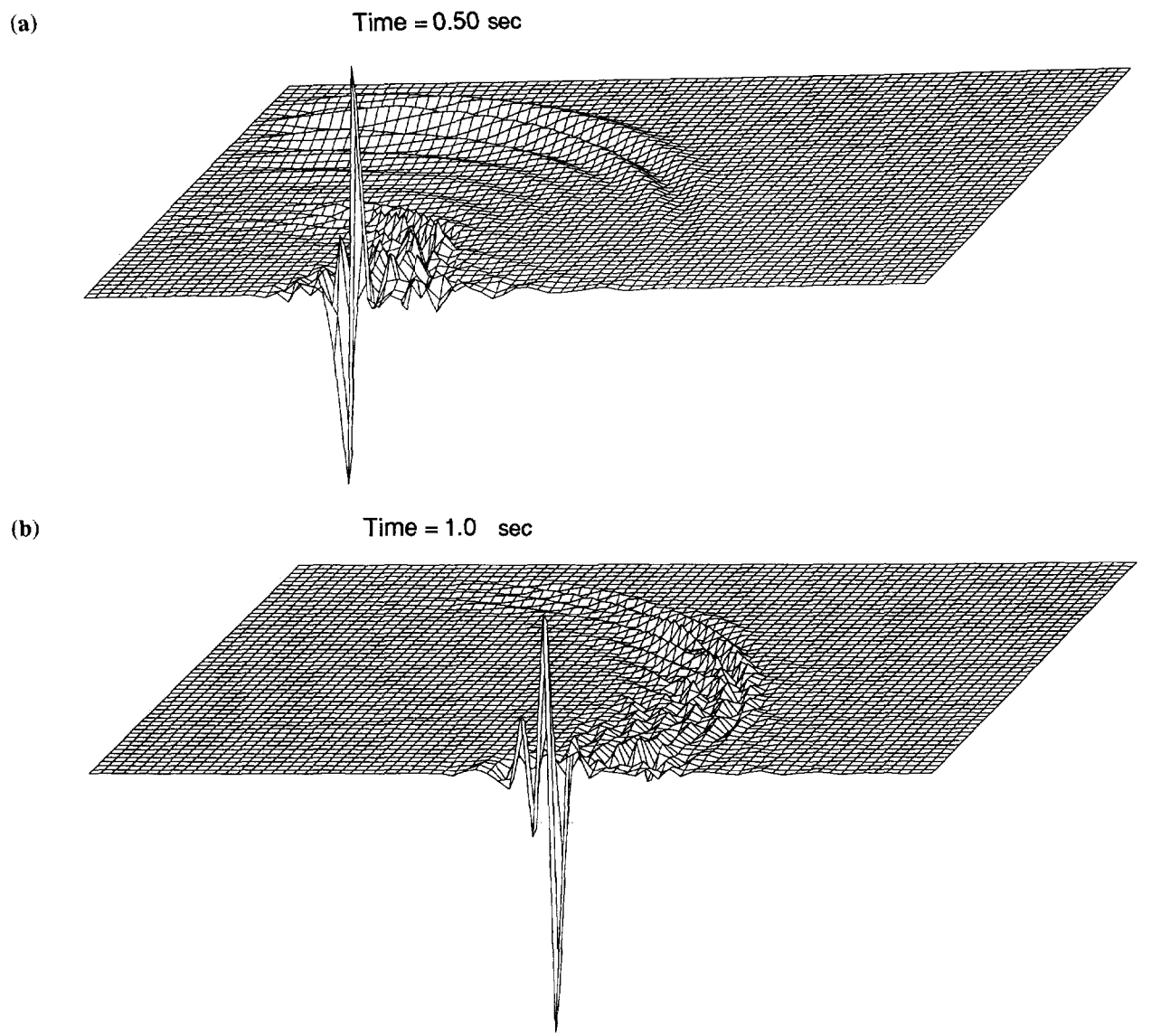

FIG. 11. Vertical particle velocity snapshots for the thin-layer problem, at times (a) $t = 0.5$ s, (b) $t = 1$ s.

α and β are two parameters which need to be specified. The derivative (dz/dy) is then given by

$$\frac{dz}{dy} = (1 + bz + cz^2)^{1/2}.$$

It can be shown that at $z = -1$, $(dz/dy) = \alpha^{-1}$, and at $z = 1$, $(dz/dy) = (\alpha\beta)^{-1}$. Thus α represents the amount of grid stretching at the boundary $z = -1$ while the grid size at $z = 0$ remains unchanged, whereas $\alpha\beta$ indicates the stretching at the other end. In addition, the grid of the y system is rescaled to have the largest grid spacing allowed by sampling considerations. By taking α proportional to the grid size N, one obtains a constant grid size in the vicinity of the boundary. In the following examples values of $\alpha = 0.06\ N$ and $\beta = 2$ were used. The resulting time step size was that which would normally be used with the Fourier method for the same temporal integration scheme.

EXAMPLE 1: LAMB'S PROBLEM

In this example of wave propagation in two-dimensional uniform half-space bounded by a free surface we compare numerical results to an analytic solution based on Cagniard's technique (Burridge, 1976). The P-wave and S-wave velocities of the medium were 3000 m/s and 500 m/s, respectively, corresponding to a Poisson's ratio of 0.473. The grid size was 225 in the horizontal direction and 161 in the vertical direction with $dx = dy = 10$ m, where dy is the largest vertical grid spacing (Figure 2). A vertical point force was applied at one grid point beneath the surface at the 25th grid line at a depth of 0.9 m. The source had a Ricker wavelet time history with a high-cut frequency of 22 Hz (or, equivalently, a peak frequency at 11 Hz), which is approximately the same frequency band which would normally be used with the Fourier method. The calculations were carried out to a time of 2 s with a time step size of 1 ms. Absorbing boundary regions were used along the bottom and sides of the numerical mesh. The absorbing regions contained 18 points (Kosloff and Kosloff, 1986).

Figures 3a and 3b compare numerical and analytical horizontal displacement time histories for points 0.9 m beneath the free surface at horizontal distances from the source of 50 m and 700 m, respectively. Figure 3c presents a comparison at a point at a depth of 360 m at a horizontal distance of 200 m from the source. The agreement between numerical and analytical solutions is very good. A similar comparison for the vertical displacements (Figures 4a–4c) is of equal quality.

EXAMPLE 2: TWO SOLIDS IN PLANAR CONTACT

This example examines the capability of the Chebychev algorithm to handle sharp velocity contrasts. The structure

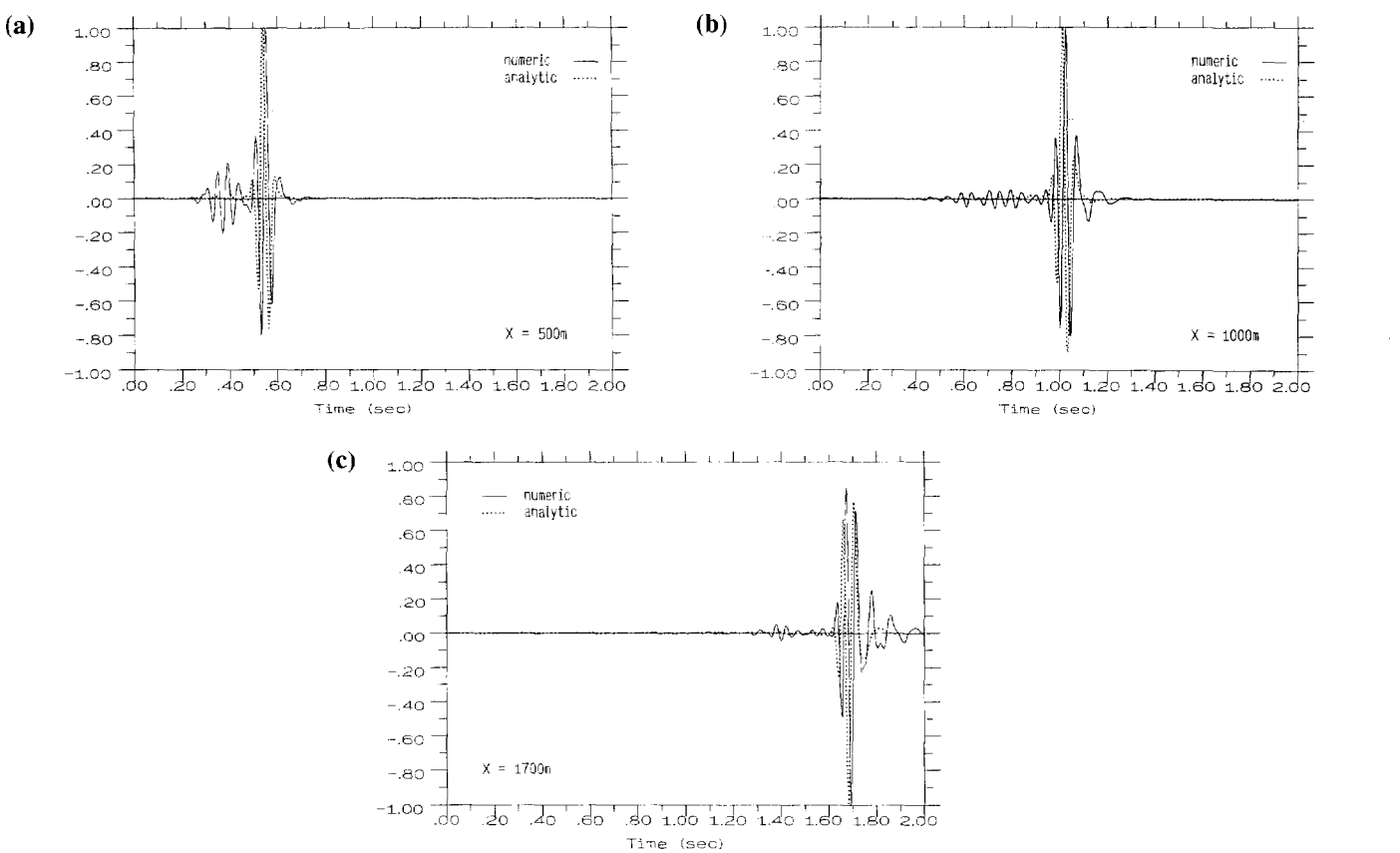

FIG. 12. Comparisons between numerical and analytical horizontal displacement solutions for the thin-layer problem at a depth of 0.9 m, (a) at a horizontal distance of 500 m from the source, (b) at a horizontal distance of 1000 m from the source, and (c) at a horizontal distance of 1700 m from the source.

consists of two different elastic regions separated by a horizontal interface (Figure 5). The material parameters were V_P = 2000 m/s, V_S = 1155 m/s, and ρ = 1.2 g/cm^3 for the medium with the source, and V_P = 3000 m/s, V_S = 1500 m/s, and ρ = 2.3 g/cm^3 for the lower medium. The calculations used the same grid as in the previous example. The shot was located 66 m above the interface and had a Ricker wavelet time history with a high-cut frequency of 42 Hz. The time step size was 1 ms and the calculations were carried out to 2 s.

Figures 6a–6c represent vertical particle velocity snapshots at respective times of 0.25 s, 0.5 s, and 1 s. In Figure 6a, which is at an early time, only the reflected and transmitted P wavefronts are well developed. However, a Stoneley wave with a large amplitude on the interface can be seen, too. In Figure 6b, both P and S reflected pulses are distinguishable. In addition, a P head wave characterized by a planar wavefront is also present. In Figure 6c the reflected P-wave has practically passed by and been absorbed along the boundaries, and a strong surface multiple can be observed propagating downward.

Figures 7a–7b and Figures 8a–8c present single-trace comparisons between numerical results and an analytical solution for two solids based on Cagniard's technique. The receiver locations are shown in Figure 5. The comparison between the solutions for the layer reflection events is very good. However, because the analytical solution does not include free-surface reflections, these are present only in the numerical results at later times.

EXAMPLE 3: A THIN LOW-VELOCITY LAYER

This problem considers wave propagation in a structure consisting of a thin horizontal layer overlying a uniform elastic half-space (Figure 9). The material parameters of the layer were P-wave and S-wave velocities of 2000 m/s and 1155 m/s, respectively, and a density of 1.2 g/cm^3. The

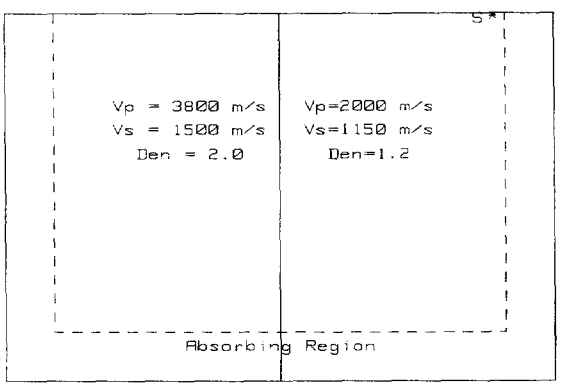

FIG. 14. Grid configuration for the vertical interface problem.

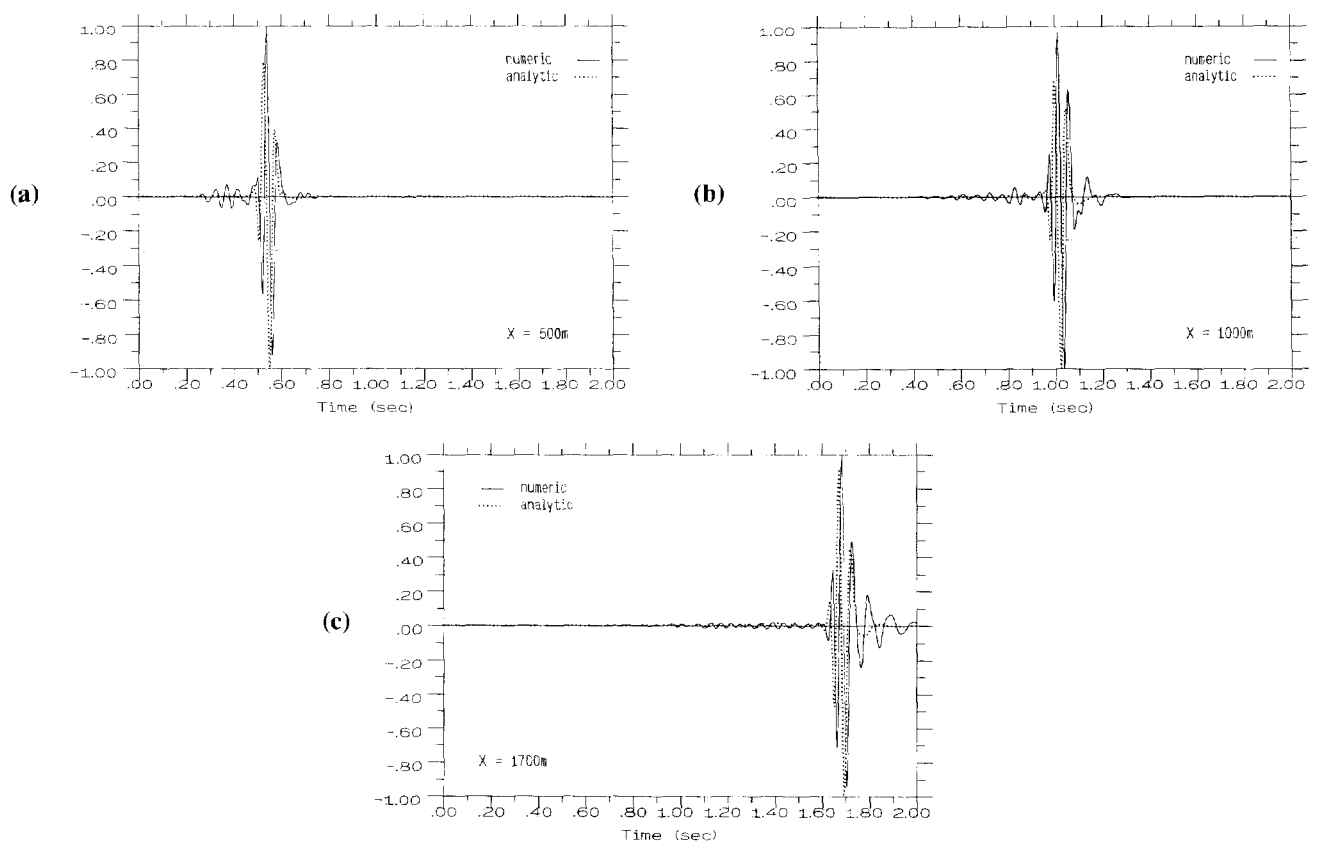

FIG. 13. Comparisons between numerical and analytical vertical displacement solutions for the thin-layer problem at a depth of 0.9 m (a) at a horizontal distance of 500 m from the source, (b) at a horizontal distance of 1000 m from the source, and (c) at a horizontal distance of 1700 m from the source.

half-space parameters were velocities of 3000 m/s and 1500 m/s and a density of 2.0 g/cm^3. The layer thickness was 60 m. A vertical point force was applied at one grid point beneath the surface at a depth of 0.9 m and at a horizontal position of 25 grid points from the boundary. The grid, source time history, time-step size, and total time were the same as in the previous example.

Figure 10a presents a horizontal displacement time section at a depth of 0.9 m. The structure of this example generates strongly dispersive surface waves which appear as a series of trapped multiples followed by the main Rayleigh wave. This can also be seen in the vertical particle velocity snapshots, Figures 11a and 11b. In these figures the body waves consist of progressing cylindrical wavefronts which can be followed azimuthally, except in the vicinity of the free surface where the phase is changed. For comparison, Figure 10b presents a time section calculated analytically based on the propagator matrix approach (e.g., Aki and Richards, 1980). The time section appears similar to Figure 10a, except that some multiples with P-wave velocity moveout are absent from it.

A detailed comparison of single traces of horizontal and vertical displacements is shown in Figures 12a–12c and Figures 13a–13c, respectively. The numerical and analytical results appear close, although the fit is not as good as in the previous examples. This may be because the analytical calculation does not account for body waves, which do have significant amplitudes, in particular at times earlier than the arrival time of the main Rayleigh pulse (Figures 11a and

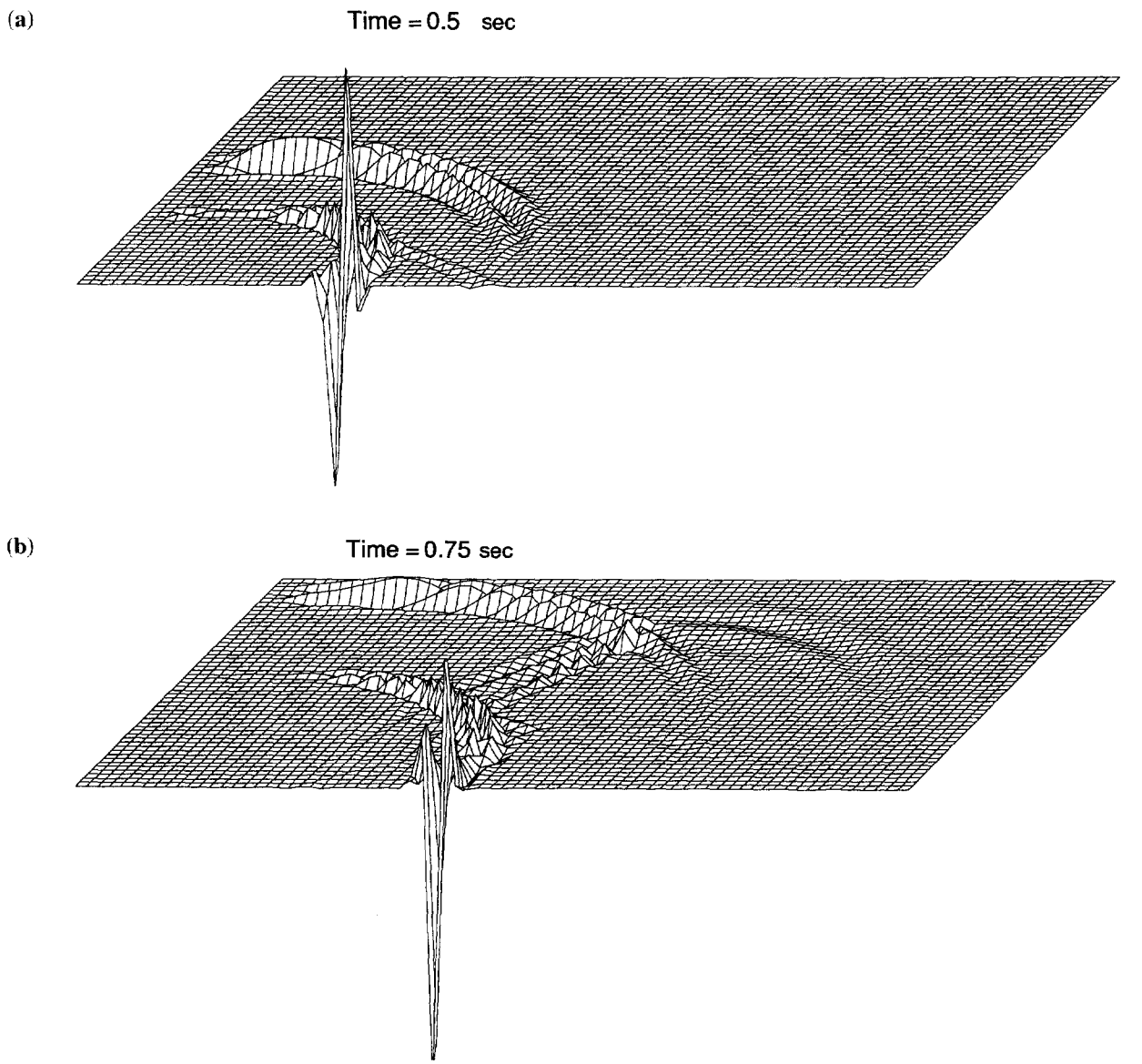

FIG. 15. Vertical particle velocity snapshots for the vertical interface problem, at times (a) t = 0.5 s, (b) t = 0.75 s, (c) t = 1 s, and (d) t = 1.25 sec.

11b). In addition, the seismograms are very sensitive to small changes in layer thickness (in numerical calculations there is always an uncertainty to within a grid spacing as to where the exact layer boundaries are).

EXAMPLE 4: A STRUCTURE WITH A VERTICAL INTERFACE

The structure in this example consists of two elastic regions separated by a vertical interface (Figure 14). The grid, source location, source time history, and time-step size were the same as in the previous example. This problem serves as a test of the modeling algorithm when all the material parameters vary laterally.

Figures 15a–15d present vertical particle velocity snapshots at times 0.5 s, 0.75 s, 1.0 s, and 1.25 s, respectively. In Figure 15a the waves have not yet reached the interface and the solution is the same as for a uniform half-space. Unlike in the previous example, the pulses appear sharp and the Rayleigh wave is nondispersed. In Figure 15b, the P wavefront has already reached the vertical interface and generated reflected and transmitted P and S wavefronts. In Figures 15c and 15d transmitted and reflected Rayleigh waves can be seen, as well as many other phases. Interestingly, Figure 15d shows that the collision with the vertical interface created a Stonely wave traveling downward along the interface.

Figure 16 presents a horizontal displacement time section collected at a depth of 0.9 m beneath the surface. The incident, reflected, and transmitted Rayleigh waves are most prominent in this figure. Note that the Rayleigh wave impinging on the interface also created converted body waves.

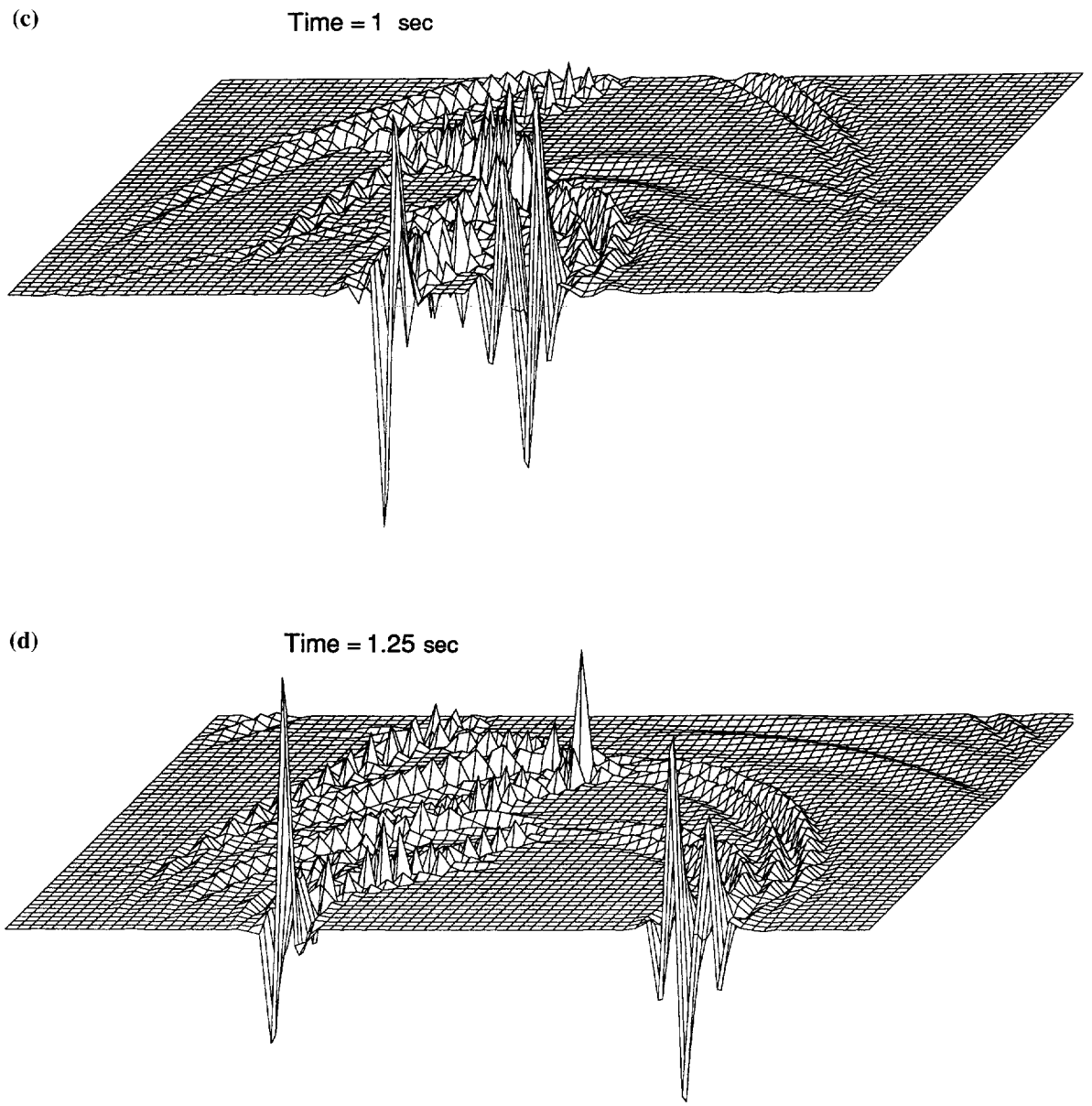

FIG. 15. Vertical particle velocity snapshots . . . continued.

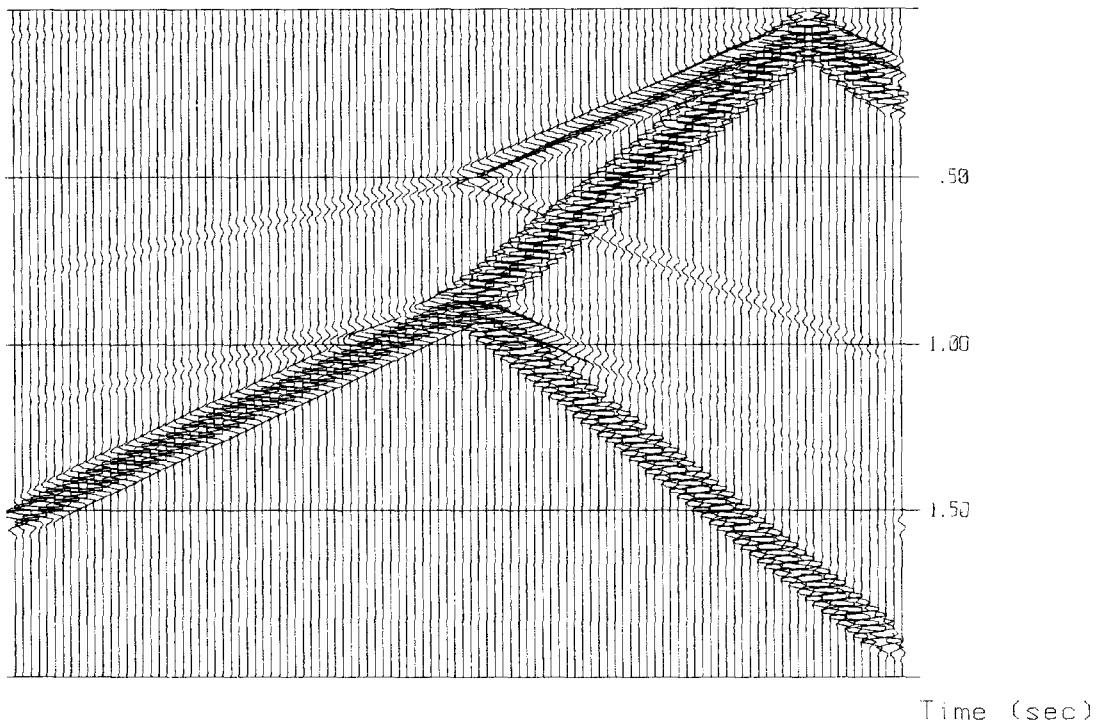

FIG. 16. Horizontal displacement time section calculated numerically for the vertical interface problem at a depth of 0.9 m.

CONCLUSIONS

We have presented a new spectral method for elastic-wave calculations which is based on a Chebychev expansion in the vertical direction. The results so far indicate that the method presents an improvement over the ordinary Fourier method in handling the free-surface boundary condition. Comparisons with analytical solutions have been good. The last example (with a vertical interface) indicates that the method can handle sharp lateral velocity contrasts across which the Poisson's ratio and density vary as well.

Compared with the efficiency of the ordinary Fourier method, the Chebychev algorithm requires more computer storage because of the need to solve the first-order system (4) and not equations (1) and (2) directly. Furthermore, the Runge-Kutta technique used in this study, for equal accuracy, is about two times slower than second-order temporal differencing which can be used with the Fourier method. It therefore appears that some price in efficiency needs to be paid when using the Chebychev scheme, but probably less than a factor of two compared to the Fourier method. Further work is needed to determine whether more accurate and efficient time integration techniques such as the Tal-Ezer method (Tal-Ezer et al., 1987) can be used with the Chebychev algorithm.

Extension of the method to more complicated material rheologies or to three spatial dimensions appears straightforward. In particular, since staggered grids are not used, complete material anisotropy can be incorporated with only minor modifications of the solution scheme.

ACKNOWLEDGMENTS

This work was supported by BMFT West Germany and the commission of the European communities. A portion of this work was done by Dan Kosloff while on a sabbatical at the Federal University of Bahia, Salvador, Brazil. Tamar Ravid participated in writing the surface wave program. Finally, we wish to thank anonymous reviewers whose comments helped improve the manuscript significantly. Computing time was provided by Convex.

REFERENCES

Aki, K., and Richards, P., 1980, Quantitative seismology: W. H. Freeman and Co.

Bayliss, A., Jordan, K. E., LeMesurier, B. J., and Turkel, E., 1986, A fourth-order accurate finite-difference scheme for the computation of elastic waves. Bull. Seis. Soc. Am., **76**, 1115–1132.

Burridge, R., 1976, Some mathematical topics in seismology: Courant Inst. of Mathematical Sciences.

Canuto, C., Hussaini, M. Y., Quarteroni, A., and Zang, T., 1987, Spectral methods in fluid dynamics: Springer-Verlag.

Cerjan, C., Kosloff, D., Kosloff, R., and Reshef, M., 1985, A nonreflecting boundary condition for discrete acoustic and elastic wave equations: Geophysics, **50**, 705–708.

Fung, Y. C., 1965, Foundations of solid mechanics: McGraw-Hill Book Co.

Gazdag, J., 1981, Modeling of the acoustic wave equation with transform methods: Geophysics, **46**, 854–859.

Gottlieb, D., Gunzberger, M. D., and Turkel, E., 1982, On numerical boundary treatment for hyperbolic systems: SIAM J. Numer. Anal., **19**, 671–682.

Gottlieb, D., and Orszag, S., 1977, Numerical analysis of spectral methods, theory and applications: Society for Industrial and Applied Mathematics.

Hamming, R., 1978, Numerical methods for scientists and engineers: McGraw-Hill Book Co.

Kosloff, D., and Baysal, E., 1982, Forward modeling by a Fourier method: Geophysics, **47**, 1402–1412.
Kosloff, D., Reshef, M., and Loewenthal, D., 1984, Elastic wave calculations by the Fourier method: Bull. Seis. Soc. Am., **74**, 875–891.
Kosloff, R., and Kosloff, D., 1986, Absorbing boundaries for wave propagation problems: J. Comp. Phys., **63**, 363–376.
Kosloff, D., and Tal-Ezer, H., 1989, Modified Chebychev pseudospectral method with $O(N^{-1})$ time step restriction: J. Comp. Phys., submitted.
Levander, A. R., 1988, Fourth-order finite-difference *P-SV* seismograms: Geophysics, **53**, 1425–1436.
Press, W. H., Flannery, B. P., Teukolski, S. A., and Veterling, W. T., 1986, Numerical recipes, The art of scientific computing: Cambridge Univ. Press.
Tal-Ezer, H., Kosloff, D., and Koren, Z., 1987, An accurate scheme for seismic forward modeling: Geophys. Prosp., **35**, 479–490.
Vidale, J. E., and Clayton, R. W., 1986, A stable free-surface boundary condition for two-dimensional elastic finite-difference wave simulation: Geophysics, **51**, 2247–2249.
Virieux, J., 1986, *P-SV* wave propagation in heterogeneous media: Velocity-stress finite-difference method: Geophysics, **51**, 889–901.